

Bio-inspired Pursuit with Autonomous Hovercraft using Lyapunov-Based Control

Daigo Shishika¹, Justin K. Yim² and Derek A. Paley³

Abstract—The problem of pursuit has been studied mostly in the context of missile guidance and navigation, however, it is also an essential component in biological systems ranging from prey capture to mating and in bio-inspired engineering applications with small, cheap, and agile vehicles. We consider the pursuit problem with a focus on robustness to noisy sensor measurements and efficiency in the control effort. We design a pursuit law based on Lyapunov analysis and establish its robustness to unknown target acceleration and measurement errors using the concept of ultimate boundedness. We also present the results from experiments conducted to study the practical challenges involved in pursuit by lightweight platforms with noisy sensors. These experiments highlight the benefit of using less control effort in the presence of large measurement errors as compared to existing missile guidance laws.

I. INTRODUCTION

Historically, pursuit has been studied mainly for the purpose of missile guidance and navigation, where it was shown that a viable approach to target intercept is stabilizing the line of sight (LOS), i.e., the line extending from the pursuer to the target [1]. Various approaches have been taken with differing assumptions [2][3][4][5], including a non-maneuvering target, lateral acceleration only (constant speed), linearized dynamics, initially negative range rate, and measurements of target acceleration.

Pursuit is also an important component in biological systems, ranging from prey capture to mating [6][7]. Stabilization of the LOS has also been studied in this context and is called motion camouflage pursuit [8]. Animals like bats [6] and insects[9] execute pursuit with limited sensor accuracy using highly agile motion. These characteristics are especially pertinent to the bio-inspired pursuit problem using small, cheap robotic vehicles.

This paper presents the design of a robust pursuit law that is inspired by the pursuit behavior of flying insects. Two closely related pursuit studies used a sliding-mode controller [10] and a partial-stability-based controller [11]. Therefore, we design a bio-inspired pursuit law with a Lyapunov-based approach fortified by the concept of ultimate boundedness.

¹Daigo Shishika is a graduate student in the Department of Aerospace Engineering, University of Maryland, 20742 MD College Park, USA daigo.shishika@gmail.com

²Justin K. Yim is a graduate student in the Department of Computer and Information Science, University of Pennsylvania, 19104 PA Philadelphia, USA yimj@seas.upenn.edu

³Derek A. Paley is the Willis H. Young Jr. Associate Professor of Aerospace Engineering Education in the Department of Aerospace Engineering and the Institute for Systems Research, University of Maryland, 20742 MD College Park, USA dpaley@umd.edu

J. K. Yim was supported by the NSF REU Grant No. 1062885.



Fig. 1. Autonomous pursuer hovercraft with onboard camera (left), and target hovercraft with IR light tower (right).

The first criterion of bio-inspired pursuit is the control effort. In small vehicles—like insects—the available control effort is restricted because of limited payload capacity, actuator size, and power/energy storage. Also, unlike missiles whose task ends at the target intercept, these pursuers may have to continue other tasks after intercept. Therefore, achieving target capture with low energy consumption is significant.

Another criterion is robustness to uncertainties like sensor noise. The measurement errors of pertinent states like range, range rate, and LOS angular rate are often ignored in the missile guidance problem. However, measurement error is an important consideration for low-cost vehicles with rudimentary sensors.

The third performance criterion arises in a near-miss scenario, i.e., how does the pursuer behave if the pursuit continues after a near miss? The effect of uncertainties due to wind, losing sight of the target, or an unexpectedly fast target maneuver may be sufficiently large that the pursuit could fail. An important strategy then is to remain close to the target after each close encounter in order to decrease the control effort for the next attempt. The same scenario also applies if the objective of the pursuer vehicle is not to capture the target but merely to stay close to it. In this case the pursuer may be required to continue the pursuit for a longer duration of time.

Existing guidance laws derived with strong assumptions have proven to be useful for real missile implementation [1], but we are not aware of any prior experimental validation of a missile pursuit law with small, cheap, and/or agile vehicles. Experiments with heterogeneous teams of ground and aerial vehicles have been conducted for pursuit-evasion games [12], however our focus is on terminal guidance. We constructed an experimental testbed using custom-built, autonomous hovercraft with onboard sensing and control (see

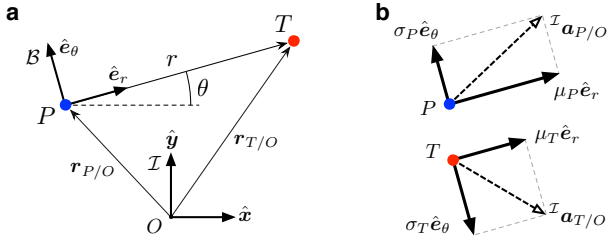


Fig. 2. (a) The definition of line-of-sight (LOS) frame \mathcal{B} and the coordinate system (r, θ) where the pursuer P is pursuing the target T . (b) Decomposition of the acceleration into radial component μ and normal component σ in LOS frame.

Fig. 1). Hovercraft are suitable to replicate flight conditions in two dimensions because unlike most wheeled vehicles they are holonomic and capable of rapid acceleration. These features make the hovercraft testbed a suitable preliminary step towards implementation of three-dimensional pursuit in flight.

The contributions of this paper are (1) a pursuit law that performs well in the near-miss scenario, is robust to measurement errors, and has less energy consumption than existing robust pursuit laws; (2) experimental demonstration of the performance of the pursuit law with a custom-built hovercraft testbed; and (3) analytical, numerical, and experimental comparison with existing pursuit laws. This paper advocates replacing pursuit laws developed for missile guidance with a bio-inspired algorithm designed for small, cheap and agile robotic vehicles.

Section II formulates the problem and introduces the basic specifications of the experimental testbed. Section III derives a bio-inspired pursuit law using Lyapunov-based control and compares it with existing pursuit laws from missile guidance. Section IV presents experimental results using an autonomous hovercraft testbed. Section V summarizes the paper and ongoing and future work.

II. BACKGROUND

A. Problem Formulation

Consider the following formulation of the pursuit problem as a planar system of two point particles with unit mass. Fig. 2 depicts the relevant reference frames and coordinates: the inertial frame $\mathcal{I} \triangleq (O, \hat{e}_x, \hat{e}_y, \hat{e}_z)$, the LOS frame $\mathcal{B} \triangleq (P, \hat{e}_r, \hat{e}_\theta, \hat{e}_z)$, the relative position vector $\mathbf{r} = \mathbf{r}_{T/O} - \mathbf{r}_{P/O}$, the range r , and the LOS angle θ . Let subscripts T and P denote the target and the pursuer, respectively.

The inertial kinematics of the two-particle system are

$$\left[\frac{\mathcal{I} d^2}{dt^2} \mathbf{r} \right]_{\mathcal{B}} = \begin{bmatrix} \ddot{r} - r\dot{\theta}^2 \\ 2\dot{r}\dot{\theta} + r\ddot{\theta} \end{bmatrix}_{\mathcal{B}} = \begin{bmatrix} \mu_T - \mu_P \\ \sigma_T - \sigma_P \end{bmatrix}_{\mathcal{B}} \quad (1)$$

where μ and σ denote the radial and normal components of the accelerations in the LOS frame.

The states of the system are defined as $\mathbf{x} = [x_1, x_2, x_3]^T \triangleq [r, \dot{r}, r\dot{\theta}]^T$. The input to the system is the relative acceleration between T and P , $\mathbf{u} = [\mu, \sigma]^T \triangleq \mathbf{u}_T - \mathbf{u}_P$ where $\mathbf{u}_T \triangleq$

$[\mu_T, \sigma_T]^T$ and $\mathbf{u}_P \triangleq [\mu_P, \sigma_P]^T$. Noting that $x_1 > 0$, we have the following state-space system on the domain $\mathcal{D} = \mathbb{R}^+ \times \mathbb{R}^2$:

$$\begin{aligned} \dot{\mathbf{x}} &= \mathbf{f}(\mathbf{x}) + \mathbf{g}(\mathbf{x})\mathbf{u}, \\ \mathbf{f}(\mathbf{x}) &= \begin{bmatrix} x_2 \\ x_3^2/x_1 \\ -x_2x_3/x_1 \end{bmatrix}, \quad \mathbf{g}(\mathbf{x}) = \begin{bmatrix} 0 & 0 \\ 1 & 0 \\ 0 & 1 \end{bmatrix}. \end{aligned} \quad (2)$$

Let δ be a small positive constant. The statement

$$\dot{r}(t) = x_2(t) < -\delta < 0, \quad \forall t > T \quad (3)$$

is a sufficient condition for target intercept in finite time [10]. Having a fixed LOS angle θ or, equivalently, satisfying the condition $x_3 = 0$, is known to be an efficient means of target intercept.

We seek to design a control law \mathbf{u}_P that ensures solutions of the system (2) converge to a domain $\mathcal{D}_2 = \{\mathbf{x} \mid x_2 < 0, x_3 = 0\}$. In doing so, we assume the following conditions are true:

- (A1) each particle can accelerate in an arbitrary direction;
- (A2) the pursuer particle measures the states \mathbf{x} with random errors;
- (A3) the target acceleration is unknown, but the bound $u_{\max} \triangleq \max\{\|\mathbf{u}_T\|\}$ is known; and
- (A4) the particles have finite size and collide only when x_1 is sufficiently small, so that $x_1 = 0$ does not occur.

B. Experimental Testbed

The bio-inspired pursuit law was implemented using a pair of small autonomous hovercraft shown in Fig. 1. Two hovercraft participate in each experiment—one as a pursuer and the other as a target. We considered several objectives in the design of this platform: good simulation of point-mass dynamics, i.e., full actuation and low drag; full onboard target tracking and control; sturdiness to endure possible collisions during pursuit; and a small diameter to operate in the available lab space.

Conventional hovercraft are frequently propelled by two rear-facing fans or one fan and rudders to provide forward thrust and yaw torque with a small number of fans [14][15]. However, the conventional configuration is underactuated and rotationally asymmetric, making it ill-suited to our application and simulation of point-mass dynamics. Other platforms add side-to-side thrusters to be fully actuated or use large numbers of thrusters, but these hovercraft are still rotationally asymmetric [16][17]. Stubbs et al. [18] developed a networked hovercraft platform that is fully actuated and rotationally symmetric; however, that platform uses offboard cameras for position measurements and a layout of four unidirectional thrusters for propulsion.

Each hovercraft measures 16 cm in diameter and weighs between 110 and 125 grams, depending on its configuration. Two lift fans carry the hovercraft and four unidirectional thrust fans arranged as in [18] accelerate and rotate the hovercraft. Each hovercraft carries an ATmega32u4 processor capable of running fully autonomous target tracking and pursuit. The pursuer tracks the target using an onboard infrared (IR) camera from a Wii-mote game controller and an

MPU6050 digital 6DOF IMU. The target hovercraft carries an infrared beacon consisting of two IR LED rings placed vertically three inches apart. This arrangement allows the pursuer to autonomously track the target without the use of any offboard measurements. The camera field of view is also limited to approximately 50 degrees in azimuth angle. A PID controller on the pursuer rotation centers the target in the camera field of view to ensure that it does not go out of sight.

Target range x_1 is calculated from the spacing of the IR points in the image. Range-rate x_2 is calculated by differentiating the measured range with respect to time. The angle to the target from the camera axis is differentiated to find the LOS rotation rate in the body frame with respect to time. This rate is added to the body frame rotation rate in the inertial frame as measured by the IMU to determine the LOS angular rate $\dot{\theta}$ in the inertial frame. Discrete low-pass filters are applied to all measured values in order to smooth out the discretized digital image measurements and to reject erroneous single-measurement deviations.

Both hovercraft are equipped with an Xbee wireless transceiver with which the pursuer transmits telemetry and the evader receives wireless steering commands from a ground station. The ground station uses an OptiTrack motion capture system to track the trajectories of the pursuer and evader and to control the trajectory of the evader. In addition, the ground station logs telemetry from the pursuer and matches it to motion capture data to record the performance (e.g., sensor measurements, controller output) of the pursuer. Motion capture was not used for guidance of the pursuer.

III. THEORETICAL RESULTS

This section presents a pursuit law designed using a Lyapunov-based approach and derives conditions on the control gains that guarantee robust target intercept. We modify the pursuit law to accommodate noisy measurements. Finally, we analytically and numerically compare the modified pursuit law to existing ones. The performance of the pursuit law is demonstrated by experiments described in Section IV.

A. Pursuit Law

One way to satisfy the target intercept condition (3) is to decrease x_2 as much as possible, as in [11]. Although this strategy may result in a short capture time, it requires a large control effort (see III-D). In addition, a high closing speed may be problematic in a near-miss scenario. Another approach is to drive x_2 to a negative constant $v_{cl} < 0$ representing the desired closing speed [10]. This strategy will keep x_2 at a reasonable value and eliminate the issues raised above.

Consider the positive semi-definite Lyapunov function candidate

$$\begin{aligned} V &= V_3(x_3) + V_2(x_2) \\ &= \frac{\kappa}{2}x_3^2 + \frac{1}{2}(x_2 - v_{cl})^2, \quad \kappa > 0. \end{aligned} \quad (4)$$

We first find the desired relative acceleration \mathbf{u}_{des} and then consider the actual control law \mathbf{u}_P of the pursuer.

One possible desired relative acceleration \mathbf{u}_{des} for the control Lyapunov function (4) was found previously using the knowledge of target acceleration and Sontag's formula [19], which is proved to have optimality in minimizing the integral of control effort and states. In contrast we make the pursuit law robust to uncertainties like unknown target acceleration by choosing

$$\mathbf{u}_{des} = \begin{bmatrix} -\frac{x_3^2}{x_1} - N_r(x_2 - v_{cl}) \\ \left(\frac{x_2}{x_1} - N_\theta\right)x_3 \end{bmatrix}, \quad N_r > 0, N_\theta > 0. \quad (5)$$

The feedback control (5) makes the derivative of the Lyapunov function V in (4) negative semi-definite, i.e.,

$$\dot{V} = -\kappa N_\theta x_3^2 - N_r(x_2 - v_{cl})^2 \leq 0. \quad (6)$$

The quadratic terms in (6) are convenient for analyzing the robustness of the pursuit law in the sequel. Note that \mathbf{u}_{des} is the desired relative acceleration, whereas $\mathbf{u} = \mathbf{u}_T - \mathbf{u}_P$ is the actual relative acceleration.

If the pursuit law is chosen to be $\mathbf{u}_P = \mathbf{u}_T - \mathbf{u}_{des}$, then $\mathbf{u} = \mathbf{u}_{des}$ and the closed-loop system will be stabilized to its equilibrium point $\mathbf{x}^* = [x_2^*, x_3^*]^T = [v_{cl}, 0]^T$, which ensures target capture in finite time. However, this pursuit law requires knowledge of the target acceleration \mathbf{u}_T . Therefore, we treat \mathbf{u}_T as an external disturbance Δ and consider the pursuit law

$$\mathbf{u}_P = -\mathbf{u}_{des}. \quad (7)$$

The relative acceleration achieved by (7) is $\mathbf{u} = \mathbf{u}_T - \mathbf{u}_P = \mathbf{u}_{des} + \Delta$, where Δ satisfies the condition $\Delta \equiv \mathbf{u}_T$. We consider the robustness of the controller to the disturbance Δ in the next section.

B. Robustness

Robustness of the pursuit law to unknown target acceleration was studied in [10] using sliding-mode control and in [11] using partial-stability-based control. In those studies, signum functions were employed to address the possibility of unknown target acceleration, which was treated as a matching disturbance. However, the effect of measurement error was not considered in [10] or [11]. We show here that the proposed pursuit law (7) where \mathbf{u}_{des} is given by (5) is robust to both unknown target acceleration and measurement error under a proper choice of the control gains N_r and N_θ .

As we have observed in our experimental testbed, the states x_1 , x_2 and x_3 can only be measured with some amount of noise. Let the measured (or estimated) states available to the pursuer be defined as $\mathbf{x}_{meas} \triangleq \mathbf{x} + \mathbf{e}$, where $\mathbf{e} = [e_1, e_2, e_3]^T$ denotes the measurement (or estimation) error. We make the following assumptions about the measurement error on the states, inspired by our experimental testbed:

- (A5) The error on the range measurement e_1 is ignored since it is sufficiently small compared to e_2 and e_3 ;
- (A6) $|e_i| \ll |x_i|$ for $i=1,2,3$, so the error terms that are higher than first order are ignored; and
- (A7) the magnitudes $|e_2|$ and $|e_3|$ are bounded by constants $e_2^* < |v_{cl}|$ and $e_3^* < |v_{cl}|/\sqrt{\kappa}$, respectively.

The validity of these assumptions for the experimental testbed is discussed in Section IV. Since the upper bound on the vehicle speed (which limits x_3) and the lower bound on the range (x_1) both exist in the physical implementation, we can also assume the following:

(A8) The absolute value of the LOS rate $|\dot{\theta}| = |x_3/x_1|$ is bounded by a constant $\omega > 0$.

The desired acceleration term, \mathbf{u}_{des} in (7) is implemented with the measured states \mathbf{x}_{meas} , i.e.,

$$\begin{aligned} \mathbf{u}_{\text{des}} &= \mathbf{u}_{\text{des}}(\mathbf{x}_{\text{meas}}) \\ &= \begin{bmatrix} -\frac{(x_3 + e_3)^2}{(x_1 + e_1)^2} - N_r(x_2 + e_2 - v_{cl}) \\ \left(\frac{x_2 + e_2}{x_1 + e_1} - N_\theta\right)(x_3 + e_3) \end{bmatrix}. \end{aligned}$$

Let $\tilde{x}_2 \triangleq x_2 - v_{cl}$. This changes the derivative of the Lyapunov function from (6) to

$$\begin{aligned} \dot{V} &= \dot{V}_3 + \dot{V}_2, \text{ where} \\ \dot{V}_3 &= \kappa \left(-N_\theta x_3^2 - N_\theta x_3 e_3 + \frac{x_3}{x_1} (x_3 e_2 + x_2 e_3) + x_3 \Delta_\theta \right) \\ \text{and } \dot{V}_2 &= -N_r \tilde{x}_2^2 - N_r \tilde{x}_2 e_2 - 2 \frac{x_3}{x_1} \tilde{x}_2 e_3 + \tilde{x}_2 \Delta_r. \end{aligned}$$

Proposition 1: The pursuit law (7) is robust to disturbance Δ and state measurement error \mathbf{e} if the control gains are chosen as

$$N_r > \frac{u_{\max} + \omega e_3^*}{|v_{cl}| - e_2^*}, \text{ and} \quad (8)$$

$$N_\theta > \frac{\sqrt{\kappa}(2u_{\max} + 2\omega e_2^* + \omega e_3^* + 4\kappa\omega e_3^*)}{2|v_{cl}| - 2\sqrt{\kappa}e_3^*}. \quad (9)$$

Moreover, if \mathbf{e} is ignored, the conditions simplify to

$$N_r > \frac{u_{\max}}{|v_{cl}|}, \text{ and } N_\theta > \frac{\sqrt{\kappa}u_{\max}}{|v_{cl}|}. \quad (10)$$

Proof: The detailed proof is omitted for length constraints. The outline is as follows: \dot{V}_2 can be decoupled from the x_3 dynamics by Assumption (A8). By bounding the cross terms (e.g., $\tilde{x}_2 \Delta_r \leq \frac{1}{2}(c_2 \tilde{x}_2^2 + \Delta_r^2/c_2)$, $\forall c_2 > 0$), \dot{V}_2 can be bounded as $\dot{V}_2 \leq -\rho_2(x_2 - v_{cl})^2 + D_2$, where ρ_2 and D_2 are functions of $N_r, v_{cl}, e_2^*, e_3^*$, and ω . By *ultimate boundedness* [13], the solutions of the system converge to a region $\mathcal{A}_2 = \{\mathbf{x} \mid x_2 \in (2v_{cl}, 0)\}$ if (8) is satisfied. This bound on x_2 can be used to decouple \dot{V}_3 from the x_2 dynamics. With a similar argument, the bound on x_3 at steady state is established. ■

C. Modification of the pursuit law

Although convergence to a rectangular region in $x_2 x_3$ -space provides a relaxed condition on the control gains, the required control may be large if the terms $|x_2 - v_{cl}|$ or $|x_3|$ are initially large. This problem is not restricted to the initial phase in the case of actual implementation. If the measurement error is large, it may cause erroneously large control input even when the actual states $|x_2 - v_{cl}|$ and $|x_3|$ are small.

In order to avoid this issue and to keep the acceleration command small even in the presence of measurement error, we saturate the linear terms in (5) as follows:

$$\mathbf{u}_{\text{des}} = \begin{bmatrix} -\frac{x_3^2}{x_1} - N_r' \text{sat}\left(\frac{x_2}{|v_{cl}|} + 1\right) \\ \frac{x_2 x_3}{x_1} - N_\theta' \text{sat}\left(\frac{\sqrt{\kappa}}{|v_{cl}|} x_3\right) \end{bmatrix}, \quad (11)$$

where $N_r' = N_r |v_{cl}|$, $N_\theta' = N_\theta |v_{cl}| / \sqrt{\kappa}$. Note that the saturation function terms are identical to the original linear terms when $|\tilde{x}_2| \leq |v_{cl}|$ and $|x_3| \leq |v_{cl}| / \sqrt{\kappa}$. One can show that the ultimate boundedness property still holds (omitted due to space constraints).

D. Comparison with other pursuit laws

In order to distinguish from other pursuit laws, let \mathbf{u}_A denote pursuit law (7), where \mathbf{u}_{des} is given by (11). We compare \mathbf{u}_A to the partial-stability-based controller \mathbf{u}_B [11] and the sliding-mode controller \mathbf{u}_C [10], which are also robust to unknown target acceleration and are given by

$$\mathbf{u}_B = \begin{bmatrix} \mu_B \\ \sigma_B \end{bmatrix} = \begin{bmatrix} \frac{x_3^2}{x_1} - v_{cl} x_2 + \eta_1 \\ \left(-\frac{x_2}{x_1} + N_B\right) x_3 + \eta_2 \text{sat}\left(\frac{x_3}{\varepsilon}\right) \end{bmatrix} \quad (12)$$

and

$$\mathbf{u}_C = \begin{bmatrix} \mu_C \\ \sigma_C \end{bmatrix} = \begin{bmatrix} \frac{x_3^2}{x_1} + \eta_1 \text{sat}\left(\frac{x_2 - v_{cl}}{\varepsilon}\right) \\ -(N_C + 1) \frac{x_2 x_3}{x_1} + \eta_2 \text{sat}\left(\frac{x_3}{\varepsilon}\right) \end{bmatrix}, \quad (13)$$

where $v, N_B, N_C, \varepsilon > 0$ and $\eta_1, \eta_2 > u_{\max}$. Also consider a naive controller \mathbf{u}_D whose radial acceleration is $\mu_D = \mu^* = \text{constant}$ and whose normal acceleration is $\sigma_D = \sigma_A$.

Remark 1: The pursuit law \mathbf{u}_B requires $x_2 < 0$ for initial condition [11], whereas law \mathbf{u}_A and sliding-mode control \mathbf{u}_C are robust to $x_2 > 0$. This robustness is also beneficial in the near-miss scenario where x_2 can change instantaneously from negative to positive.

Metrics often used in comparing pursuit strategies include the capture time, the required σ_P , and the required μ_P . There is no significant difference in the performance and control effort in the normal component between the considered pursuit laws, as can be seen in [11] and also in the numerical simulation shown below. Once $\dot{\theta} \approx 0$ is achieved, short capture times are achieved by using a large μ_P , as can be seen from the dynamics (2), i.e., $\dot{x}_2 = \mu_T - \mu_P$ if $x_3 = 0$. Therefore, to achieve a pursuit law with a short capture time one needs simply to command the maximum available radial acceleration. Based on these observations, we focus on the radial component and compare the minimal control effort that guarantees robust target intercept.

All of the pursuit laws except \mathbf{u}_D have the term x_3^2/x_1 , which cancels the centrifugal acceleration in \mathcal{B} . Let

$$G \triangleq \mu - \frac{x_3^2}{x_1} \quad (14)$$

denote the additional term on the radial component in order to compare G among the three pursuit laws. For a fair comparison, we choose the smallest control gains that

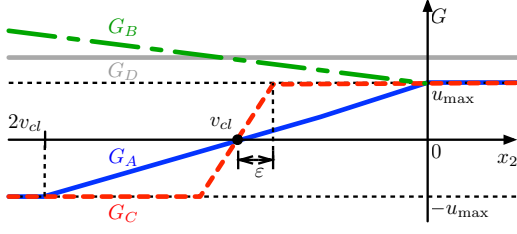


Fig. 3. Comparison of the controller specific terms G (see (14)) in the radial control as a function of range rate x_2 . For simplicity, $x_3=0$ is assumed for the naive controller G_D . The pursuit law G_A has the smallest absolute value that results in the smallest energy expenditure.

guarantee robustness (strictly speaking, the limiting value, i.e., if $N > a$ is required, then we choose $N = a$). Only the no-measurement-error case is considered since measurement error was not studied in [10][11].

From condition (10) and (11), $N'_r = u_{\max}$. The additional term G of the control laws with minimal gains are

$$\begin{aligned} G_A &= u_{\max} \text{sat} \left(\frac{x_2}{|v_{cl}|} + 1 \right) \\ G_B &= -v x_2 + u_{\max} \\ G_C &= u_{\max} \text{sat} \left(\frac{x_2 - v_{cl}}{\varepsilon} \right) \\ G_D &= \mu^* - x_3^2 / x_1. \end{aligned}$$

Fig. 3 shows G as a function of x_2 . Noting that \mathbf{u}_A ensures $\tilde{x}_2 < |v_{cl}| \Leftrightarrow 2v_{cl} < x_2 < 0$ at steady state, G_A has the smallest absolute value for the same states \mathbf{x} .

Remark 2: The sliding-mode controller μ_C becomes identical to μ_A if $\varepsilon = |v_{cl}|$. Although ε is usually a small value introduced in order to avoid the chattering from the signum function, it can be as large as $|v_{cl}|$ and still guarantee robustness.

Fig. 4 shows the results of numerical simulation up to the first close encounter. The open-loop control of the target is specified by $\mathbf{u}_T(t)=[0.5 \sin(0.4\pi t+0.3\pi), 0.5 \sin(\pi t+0.4\pi)]$ and the initial conditions are $\mathbf{r}_{P/O}(0)=[0,0]$, $\mathbf{v}_{P/O}(0)=[0,0]$, $\mathbf{r}_{T/O}(0)=[2,0]$, and $\mathbf{v}_{T/O}(0)=[-.5,.7]$. Parameters and control gains were chosen as $v_{cl}=-2.0$, $\kappa=400$, $\nu=0.1$, $N_B=0.5$, $N_C=1$, $\varepsilon=0.1$, and $u_{\max}=0.5$, which gives $N'_r=N'_\theta=\eta_1=\eta_2=0.5$. The naive control law \mathbf{u}_D is simulated with $\mu_1^* = 0.4$ and $\mu_2^* = 0.7$ denoted Naive 1 and Naive 2, respectively. We define the energy consumption as $E_{tot} = \int_{t_0}^t \|\mathbf{u}(\tau)\|^2 d\tau$ [20]. {Since the motor voltage on the hovercraft is proportional to the magnitude of the acceleration command and voltage-current relationship is close to linear in the range in which the hovercraft operates, the quadratic form of the energy estimate is valid for the hovercraft testbed.} E_μ and E_σ are the radial and normal component of the energy consumption. The normal components are all similar except at the end, when x_1 becomes small. In the radial component, the bio-inspired control law (blue) is the smallest in both maximum acceleration and energy consumption.

Fig. 5 shows the case when the pursuit is continued after the first close encounter. This corresponds to the near-miss

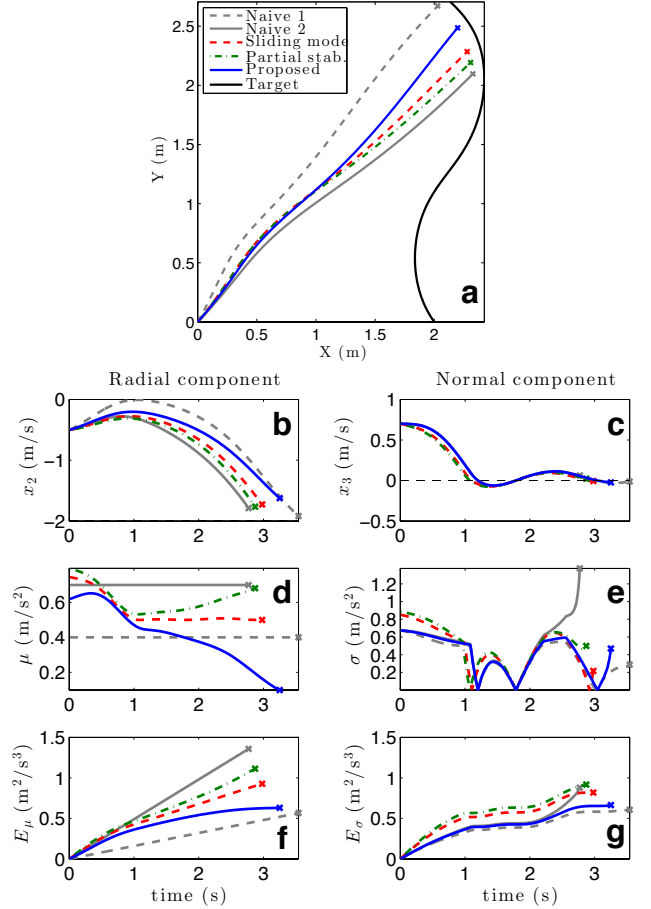


Fig. 4. Numerical simulation until the first close encounter. (a) Trajectories from different pursuit laws against the same target (black). (b, c) States. (d,e) Absolute value of acceleration commands. (f, g) Energy expenditure calculated from the time integral of squared acceleration commands. The left column (b, d, f) and the right column (c, e, g) describe the radial and normal components in LOS frame, respectively.

or the target tracking scenarios. To quantify the tracking performance, we look at the energetic cost $J = \int_0^t (x_1(\tau))^2 d\tau$, as shown in Fig. 5b. The bio-inspired pursuit law has the smallest J and the smallest energy consumption E_{tot} .

IV. EXPERIMENTAL RESULTS

The various pursuit laws described above were implemented using the autonomous hovercraft testbed. We also used a motion-capture camera system to set the vehicles to the desired initial conditions in the inertial frame, to command a repeatable trajectory for the target, and to analyze the performance of the pursuit by measuring the ground truth. Initial conditions and target trajectory identical to the numerical simulation were used.

A. Measurement Noise

Vision-based tracking like that used on the pursuer hovercraft is a low-power, light-weight tracking solution for small, payload-limited platforms. Measurements of the range and body-frame angle to the target from the pursuer are

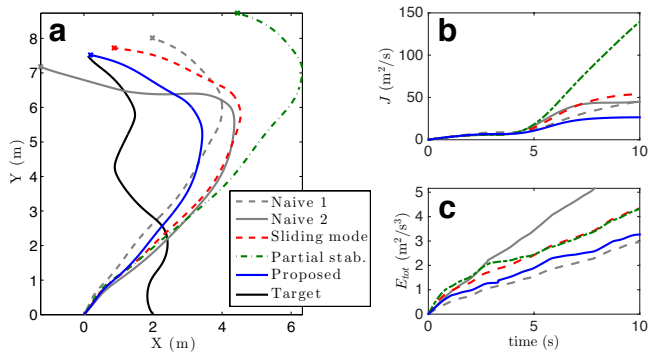


Fig. 5. Numerical simulation of continued pursuit. (a) Trajectories from different pursuit laws against the same target (black). (b) Energetic cost $J = \int_0^t x_1^2 d\tau$, which penalizes the deviation from the target. (c) The total energy expenditure E_{tot} .

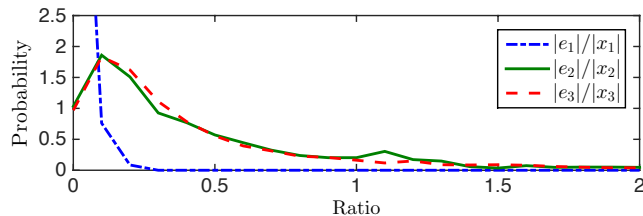


Fig. 6. Probability density of error-to-signal ratio from 18 runs.

corrupted by limited camera resolution, occasional extraneous IR sources and reflections, and other random noise. Differentiation of this noisy signal to calculate radial and angular velocity further exacerbates the high frequency noise. Table I shows the measurement errors across eighteen pursuit experiments.

Due to the generally large errors e_2 and e_3 and infrequent extreme deviations in e_3 , e_i often approaches x_i and even occasionally exceeds it, though the error-to-signal ratio is usually less than 0.5 as shown in Fig. 6. Hence, Assumption (A6) is marginally true for e_2 and e_3 . With the controller parameters $v_{cl} = -2$ and $\kappa = 10$, the magnitudes of e_2 and e_3 agree with Assumption (A7) most of the time; $|e_2| > |v_{cl}|$ and $|e_3| > |v_{cl}| / \sqrt{\kappa}$ occurs only 0.42% and 0.73% of the time steps respectively. We estimate the bounds as $e_2^* = 0.56$ m/s and $e_3^* = 0.30$ m/s using two standard deviations, which accommodates 97.6% and 95.4% of all errors. For Assumption (A8), we estimate the maximum LOS angular rate as $\omega = 1$ rad/s.

The control gains calculated from (8), (9) and (11) are $N_r' = 1.1$ and $N_\theta' = 12.4$; $N_r'' = N_\theta'' = 0.5$ from (10) when measurement error is ignored. Although the mean capture time from 10 experimental runs increased from 2.7 sec with the

TABLE I
CHARACTERISTICS OF THE STATE MEASUREMENT ERRORS

	Units	Mean	S.D.	Max.
e_1	m	0.023	0.031	0.14
e_2	m/s	0.112	0.289	2.26
e_3	m/s	-0.002	0.151	3.15

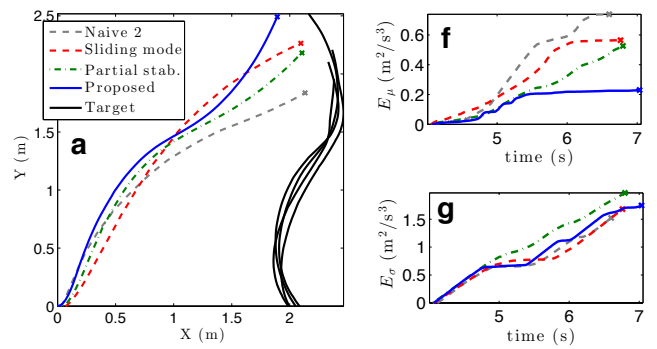


Fig. 7. Experimental run with hovercraft until the first close encounter. Subfigures f and g correspond to those in Fig. 4.

former control gains to 3.2 sec with the latter control gains, robust target capture was still achieved with the smaller gain setting, which implies that the gain condition that is robust to measurement error may be conservative for this testbed.

B. Comparison between Pursuit Laws

As in the numerical simulations, we ran each controller against a pre-programmed target trajectory and recorded the pursuer's trajectory, onboard state measurements, and control effort. The parameters and control gains were identical to those in the numerical simulations. Fig. 7 shows the results from conducting identical experimental trials for each law. We characterize controller performances by capture time, maximum control effort, and energy expenditure. As in Section III, we are most interested in the maximum control effort and energy expenditure since both the control authority and energy stores are particularly limited on small autonomous vehicles. Each controller was run three times and the average of each of the above metrics is listed in Table II. The symbols μ_{max} , U_{max} , E_μ , E_{tot} and T_{cap} denote maximum radial acceleration command, maximum acceleration command, radial energy expenditure, total energy expenditure, and capture time, respectively. Note that μ_{max} and U_{max} are the values before the saturation at 1 m/s^2 . The bio-inspired controller has the smallest acceleration and energy expenditures and the longest capture time. The naive pursuit law has the shortest capture time and the largest energy expenditure.

C. Comparison with Theory

Our experimental pursuit implementation revealed several insights when compared to analytical and numerical results.

First, the experiments provide a realistic baseline for noise in small, low-cost, vision-based sensors used in pursuit. As

TABLE II
PERFORMANCES OF DIFFERENT PURSUIT LAWS

	μ_{max} (m/s ²)	U_{max} (m/s ²)	E_μ (m ² /s ³)	E_{tot} (m ² /s ³)	T_{cap} (s)
Proposed	0.81	3.70	0.25	1.82	3.16
Partial stab.	1.18	5.46	0.52	2.48	2.90
Sliding mode	1.13	6.63	0.68	2.03	2.88
Naive	0.80	6.70	0.79	2.37	2.75

expected, differentiated rate measurements like x_2 and x_3 are significantly noisier than direct range or angle measurements like x_1 , when using vision sensors such as the camera on the pursuer. Though the magnitude of the noise, specifically in x_2 and x_3 , violated the theoretical assumptions, the controllers' success demonstrate that a well-designed controller can reliably achieve target capture outside of the guaranteed operating regime.

Second, actuator saturation due to limited actuator authority changed controller performance as compared to simulation, emphasizing the importance of a low maximum commanded acceleration. Since no bound is assumed on pursuer acceleration in the controller derivations, unachievable acceleration magnitudes can be commanded. This problem is exacerbated by sensor noise, which can produce erroneously large state measurements and corresponding large fluctuations in acceleration commands. In the experimental implementation, overly large acceleration commands are saturated by scaling down to the maximum achievable acceleration magnitude while maintaining the original direction. In particular, this modified the achieved acceleration when either μ or σ command exceeded the maximum acceleration magnitude. The effects of actuator limits could be avoided or mitigated by limiting the maximum commanded acceleration or by different scaling and saturating strategies when unachievable accelerations are commanded.

V. CONCLUSION

Inspired by the pursuit behavior of flying insects, we considered low-energy consumption, robustness to uncertainty, and performance in the near-miss scenario to design a bio-inspired pursuit law for small, cheap, and agile robotic vehicles using Lyapunov-based control. We performed analytical, numerical, and experimental comparison of various pursuit laws and showed that the bio-inspired pursuit law has the least energy consumption among considered pursuit laws while staying close to the target in the near-miss scenario.

The experiments showed that the magnitude of measurement error is not negligible. We used Lyapunov analysis together with an ultimate boundedness condition to establish the robustness of the new pursuit law to unknown target acceleration and measurement error. However, the experiments also showed that the gain condition for the robustness is conservative, which may have been caused by the deterministic analysis of the error bounds. In ongoing work, we are considering three-dimensional pursuit and a stochastic approach to model the effect of measurement error.

ACKNOWLEDGMENT

We thank Jonathan Fiene, University of Pennsylvania Mechanical Engineering and Applied Mechanics for providing us with cameras used in the hovercraft. The authors would also like to acknowledge valuable discussions with Derrick Yeo and Frank Lagor related to this work.

REFERENCES

- [1] P. Zarchan. Tactical and strategic missile guidance. *Progress in astronautics and aeronautics*, 176, 2002.
- [2] F.W. Nesline and P. Zarchan. A new look at classical vs modern homing missile guidance. *Journal of Guidance, Control, and Dynamics*, pages 78–85, 1981.
- [3] S.N. Ghawghawe and D. Ghose. Pure proportional navigation against time-varying target manoeuvres. *IEEE Transactions on Aerospace and Electronic Systems*, 32(4):1336–1347, 1996.
- [4] P. Gurfil. Non-linear missile guidance synthesis using control Lyapunov functions. *Proceedings of the Institution of Mechanical Engineers, Part G: Journal of Aerospace Engineering*, 219(2):77–87, January 2005.
- [5] Y.B. Shtessel. Guidance and control of missile interceptor using second-order sliding modes. *IEEE Transactions on Aerospace and Electronic Systems*, 45(1):110–124, 2009.
- [6] K. Ghose, T.K. Horiuchi, P.S. Krishnaprasad, and C.F. Moss. Echolocating bats use a nearly time-optimal strategy to intercept prey. *PLoS biology*, 4(5):865–873, May 2006.
- [7] W. Scott and N.E. Leonard. Pursuit, herding and evasion: A three-agent model of caribou predation. *American Control Conference*, (1):2984–2989, 2013.
- [8] E.W. Justh and P.S. Krishnaprasad. Steering laws for motion camouflage. *Proceedings of the Royal Society A: Mathematical, Physical and Engineering Sciences*, 462(2076):3629–3643, December 2006.
- [9] Abdoulaye Diabaté, Alpha S Yaro, Adama Dao, Moussa Diallo, Diana L Huestis, and Tovi Lehmann. Spatial distribution and male mating success of *Anopheles gambiae* swarms. *BMC evolutionary biology*, 11(1):184, January 2011.
- [10] J. Moon, K. Kim, and Y. Kim. Design of missile guidance law via variable structure control. *Journal of Guidance, Control, and Dynamics*, 24(4):659–664, July 2001.
- [11] T. Binazadeh and M.J. Yazdanpanah. Robust partial control design for non-linear control systems: a guidance application. *Proceedings of the Institution of Mechanical Engineers, Part I: Journal of Systems and Control Engineering*, 226(2):233–242, September 2012.
- [12] R. Vidal and O. Shakernia. Probabilistic pursuit-evasion games: theory, implementation, and experimental evaluation. *IEEE Transactions on Robotics and Automation*, 18(5):662–669, 2002.
- [13] H.K. Khalil and J.W. Grizzle. *Nonlinear Systems*. Upper Saddle River: Prentice hall, 2002.
- [14] K. Tanaka, M. Iwasaki, and H.O. Wang. Switching control of an R/C hovercraft: stabilization and smooth switching. *IEEE transactions on systems, man, and cybernetics. Part B, Cybernetics : a publication of the IEEE Systems, Man, and Cybernetics Society*, 31(6):853–863, January 2001.
- [15] S.B. Fuller and R.M. Murray. A hovercraft robot that uses insect-inspired visual autocorrelation for motion control in a corridor. *2011 IEEE International Conference on Robotics and Biomimetics*, pages 1474–1481, December 2011.
- [16] F.L. Roubieu, J. Serres, N. Franceschini, F. Ruffier, and S. Viollet. A fully-autonomous hovercraft inspired by bees: Wall following and speed control in straight and tapered corridors. *2012 IEEE International Conference on Robotics and Biomimetics (ROBIO)*, pages 1311–1318, December 2012.
- [17] C. Detweiler, B. Griffin, and H. Roehr. Omni-directional hovercraft design as a foundation for MAV education. *2012 IEEE/RSJ International Conference on Intelligent Robots and Systems*, pages 786–792, October 2012.
- [18] A. Stubbs, V.I. Vladimerou, A.T. Fulford, D. King, and J. Strick. A Hovercraft Testbed for Networked and Decentralized Control. *IEEE Control Systems Magazine*, 26(3):56–69, 2006.
- [19] C. Ryoo, Y. Kim, M. Tahk, and K. Choi. A missile guidance law based on Sontag's formula to intercept maneuvering targets. *International Journal of Control, Automation, and Systems*, 5(4):397–409, 2007.
- [20] Y. Guo, S. Wang, Y. Yao, and B. Yang. Evader maneuver on consideration of energy consumption in flight vehicle interception scenarios. *Aerospace Science and Technology*, 15(7):519–525, 2011.